Advances in Aircraft and Spacecraft Science, *Vol. 10, No. 4 (2023) 317-334*
https://doi.org/10.12989/aas.2023.10.4.317

Paraffin-based ramjet missile preliminary design

Rogério L.V. Cruz[1], Carlos A.G. Veras*[1] and Olexiy Shynkarenko[2]

[1]*Mechanical Engineering Department, University of Brasília, Campus Darcy Ribeiro, 910-900 Brasilia-DF, Brazil*
[2]*Department of Aerospace Engineering, University of Brasília, Gama Leste, 72444-240 Brasilia-DF, Brazil*

(Received February 15, 2023, Revised July 5, 2023, Accepted July 12, 2023)

Abstract. This paper presents a basic methodology and a set of numerical tools for the preliminary design of solid-fueled ramjet missiles. An elementary code determines the baseline system configuration comprised of warhead, guidance-control, and propulsion masses and geometries from specific correlations found in the literature. Then, the system is refined with the help of external and internal ballistics codes. Equations of motion are solved for the flight's ascending, cruising, and descending stages and the internal ballistic set of equations designs the ramjet engine based on liquefying fuels. The combined tools sized the booster and the ramjet sustainer engines for a long-range missile, intended to transport 200 kg of payload for more than 300 km range flying near 14,000 m altitude at Mach 3.0. The refined system configuration had 600 mm in diameter and 8,500 mm in length with overall mass of 2,128 kg and 890 kg/m3 density. Ramjet engine propellant mass fraction was estimated as 74%. Increased missile range can be attained with paraffin-polyethylene blend burning at near constant regression rate through primary air mass flow rate control and lateral 2-D air intakes.

Keywords: aerodynamics; liquefying fuels; ramjet preliminary design; solid-fueled ramjet propulsion

1. Introduction

The Brazilian Exclusive Economic Zone, an offshore area spanning 3.6 million square kilometers, poses complex surveillance and defense challenges for the Brazilian Navy. To ensure its protection, the deployment of state-of-the-art anti-ship weaponry is necessary. As part of this effort, the Brazilian industry (AVIBRAS) is currently qualifying a long-range subsonic missile (300 km) propelled by a gas turbine jet engine (ASTROS, 2014). In addition, ongoing research is being conducted by the Institute of Aeronautics and Space (IAE) and the Institute for Advanced Studies (IEAv) to develop hypersonic technology, as discussed by Martos *et al.* (2017). While Brazil has successfully developed and operated a broad range of sounding rockets based on solid propellant technology (Garcia *et al.* 2011), the country has limited experience in developing supersonic missile technology. Furthermore, only a few academic institutions are currently working on ramjet propulsion, which cannot be commercialized or transferred between countries in compliance with the directives of the Missile Technology Control Regime (Sidhu 2007).

The University of Brasilia has been investigating ramjet and hybrid rocket propellant technology for over 20 years, as reported in Bertoldi *et al.* (2022). Recently, Shynkarenko *et al.*

*Corresponding author, Professor, E-mail: gurgel@unb.br

http://www.techno-press.org/?journal=aas&subpage=7 ISSN: 2287-528X (Print), 2287-5271 (Online)

(2019) presented a novel test bench and associated methodology designed to investigate advanced propulsion technology for rockets and ramjets. The apparatus is capable of handling various propellants, including solid paraffin, high-density polyethylene, methane, and kerosene, with high-temperature air streams (ramjets), GOx, and N_2O (rockets). The research team has also focused on the development of numerical tools for the design and optimization of long-range tactical missiles (Neiva, 2016), launch vehicles (da Cás *et al.* 2019), and other propulsion systems (da Cás *et al.* 2012). Apart from that, no published work on the open international literature has addressed the design of long-range surface-to-surface missiles based on liquefying fuels. Here, we present a set of numerical tools for the preliminary design of supersonic anti-ship missiles. A preliminary code predicts baseline missiles' main subsections extracted from published correlations. An external ballistics code integrates the trajectory equations covering the flight's ascending, cruising, and descending stages and an additional code helps design the solid-fueled ramjet sustainer. Then, through a series of refinements, these combined codes are used to identify a preliminary missile configuration that meets the system's mission requirements. The primary focus of our efforts lies in the design of the booster and the ramjet sustainer engines, with the latter being based on solid paraffin-polyethylene blends.

2. Tactical missiles and ramjet propulsion

2.1 Tactical missiles

Missiles are self-propelled guided weapons classified as strategic or tactical, depending on their purpose, type of warhead, flight range, cost, inventory, and frequency of use for combat or deterrence scenarios (Fleeman 2012). The Brazilian coastal line stretches approximately 8.5 thousand kilometers and accommodates 80% of the country's population. This narrow strip of land runs alongside the entire shoreline, encompassing sixteen out of the twenty-seven state capitals, crucial ports and airports, two rocket launch bases, as well as oil and gas complexes comprising pipelines and offshore drilling refineries. Additionally, it serves as the primary infrastructure hub for maritime routes used in international commerce. To underscore the significance of this region, the Brazilian National Defense Policy emphasizes the strategic importance of the South Atlantic region, with the Brazilian Navy designated as the leading authority responsible for safeguarding all coastal assets, as outlined in the National Strategy of Defense (Decreto 2008). Currently, Brazil is developing the MANSUP, an anti-ship subsonic missile that may have limited effectiveness against a well-defended naval task force in certain scenarios. Therefore, it is crucial to consider the development of missiles with improved range and speed to address this limitation.

As discussed in Dutta (2014), the attacking missile detection range is a function of the radar cross-section, radar height, and the ASCM flight altitude. Therefore, low altitude flight, small diameter missiles traveling at very high speed implies less time to interception, increasing the probability of hitting the targeted ship. High-speed flight ($M \geq 2.5$) at low altitude causes excessive drag forces and occurs at enormous air stagnation temperature and pressure. For such high speed, cruising stage should take place at high altitudes.

For the preliminary design, the study should focus on concepts, theory, and initial assessment that precede the industrial stage. In this work, we presume that the Brazilian Navy is the primary customer. The European Cooperation for Space Standardization (ECSS 2022) recommends splitting new projects into seven phases (0, A-F), which are planned by the main stakeholders,

ranging from top-level customers to lower-level suppliers. As the top-level customer, the Navy should define system needs and performance criteria and actively participate in the execution of preliminary studies to guide Phase-zero of the missile development life-cycle in accordance with the ECSS recommendations.

2.2 Ramjet propulsion

In a solid-fueled ramjet, the system geometry is governed by the fuel-burning regime. The fuel regression rate depends on the heat transfer from the combustion zone to the solid grain and mass transfer from the grain surface to the burning region. These processes are complex and cannot be solved analytically as reviewed in Karabeyoglu *et al.* (2004). The literature describes mechanisms and ballistic models for liquefying (paraffin) and non-liquefying polymeric fuels applied to hybrid rocket and ramjet propulsion systems. The most known of these models gives the relationship between the regression rate and oxidizer mass flux in the form of

$$\dot{r} = \frac{dr}{dt} = a\, G^n \tag{1}$$

In Eq. (1), the empirical constants (ballistic coefficients) "*a*" and "*n*" are positive and *G* is the average oxidizer mass flux through the grain port. Since the grain's port area grows during the flight, the regression rate decreases for constant oxidizer mass flow rate. The integration of the $\dot{r}$ function along engine operation determines the instantaneous average grain thickness and its final diameter. Therefore

$$D_{iam}(t) = D_{ini} + 2 \int_{t_{i,r}}^{t_{f,r}} \dot{r}\, dt \tag{2}$$

The ballistic coefficients depend on the fuel and oxidizer compositions, flow structure, and the temperature of the hot air compressed through the ramjet's supersonic diffuser. For the ramjet's typical air mass flux range of 10-350 kg/m^{2}s, the regression rate of polyethylene did not exceed 0.3 mm/s (Schulte *et al.* 1987). Motor low regression rate would claim long solid grains, penalizing the propellant mass fraction of the ramjet engine and missiles overall weight. The fuel, however, is a competitive candidate for long-range missiles since it can sustain extended operation times, as implied in Eq. (2).

Azevedo *et al.* (2019) observed regression rates in excess of 1.4 mm/s for paraffin-air combustion in an experimental ramjet motor. The high regression rate of paraffin suggests short grain lengths and reduced engine operating time, thus suitable for short-range missiles. The low melting temperature and grain mechanical strength of pure paraffin may need further assessment when applied to missile systems.

Fig. 1 shows pictures taken from the experimental test campaign conducted by Azevedo *et al.* (2019). As it can be seen the initial burn of paraffin in air takes place in lean combustion regime (Fig. 1A) as the blue clean flame (plume) suggests. Few seconds later, the combustion improves forming a bright yellow flame on account of soot radiation at high temperature. The picture also shows possible paraffin droplets emerging from the lower part of nozzle (Fig. 1B) along with unburnt gas phase by-products (smoke), despite engine overall *FA* ratio set for lean combustion. The liquid layer brought to the nozzle entrance was sprayed in a way similar to conical two-phase flow atomizers. Such fuel losses reduce overall combustion efficiency and facilitates missile

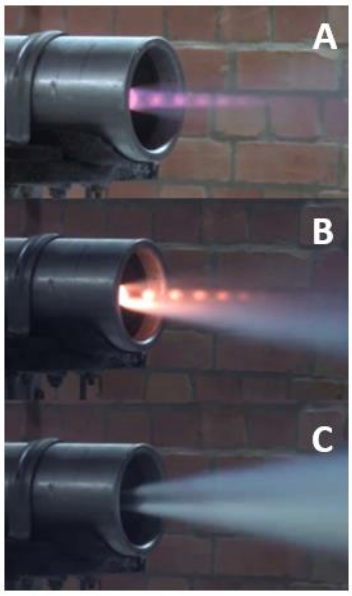

Fig. 1 Paraffin-based experimental ramjet engine at different burning stages.

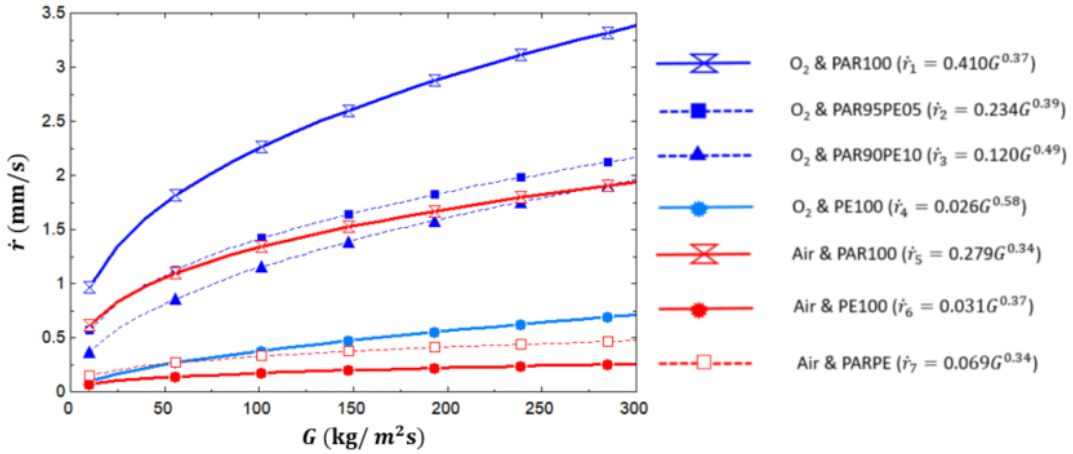

Fig. 2 Regression rate curves for different hybrid (blue) and ramjet (red) engine propellants: $\dot{r}_1$ to $\dot{r}_4$ (Kim *et al.* 2015), $\dot{r}_4$ (Azevedo et al, 2019), $\dot{r}_6$ (Schulte *et al.* 1987), and $\dot{r}_7$ (this work)

tracking. The phenomenon was even more pronounced just after combustion extinguishment, as the accumulated liquid layer at the bottom of the grain emerged from the nozzle (Fig. 1C) in the form of long paraffin jet spray. Given the unpredictable mean diameter of droplet entrainment, which contributes to the high regression rate of paraffin, it is crucial to accurately estimate the minimum length required for the motor's post-combustion chamber. This estimation is vital to ensure complete combustion and achieve optimal system performance. Applying the D^2 law (Turns 2011) for liquid droplet evaporation under air flow conditions of 1600 K and 3.0 bar pressure, the recommended post-combustion chamber length is approximately 12 mm, 50 mm, 310 mm, and 1,240 mm for initial droplet diameters of 10 μm, 20 μm, 50 μm, and 100 μm,

respectively, when issuing near the solid fuel grain exit. These predictions are conservative since the lifetime of the paraffin droplets decreases under oxidizing conditions, implying a shorter post-combustion chamber length. However, these concerns can be eliminated by choosing integrated rocket-ramjet engine technology, which offers increased residence times for droplet combustion within the system.

Fig. 2 shows regression rate curves for different pairs of propellants applied to hybrid rockets and ramjet engines. The ballistic coefficients for pure paraffin ($\dot{r}_1$), paraffin-polyethylene blends ($\dot{r}_2$ and $\dot{r}_3$), and pure polyethylene (PE100) burning with oxygen were taken from Kim *et al.* (2015). Paraffin-air and polyethylene-air ballistic data were taken from Azevedo *et al.* (2019) and Schulte *et al.* (1987), respectively. The difference in regression rates between paraffin and polyethylene is clear, whether applied to hybrid rocket or ramjet engine as shown in Fig. 2. Liquefying fuels have the additional effect of droplet entrainment caused by the melted layer instability. The entrainment rate depends on the liquid fuel properties which changes as the fuel composition is altered. Kim *et al.* (2015) reported decreased regression rate with the addition of only 5% of polyethylene in paraffin, as the curves $\dot{r}_1$ and $\dot{r}_2$ show. Further increase in the mass fraction of polyethylene ($\dot{r}_3$) had less effect in reducing the fuel regression rate. Such trends also hold when the oxidizer is air, as observed by Li *et al.* (2020) who measured regressions rates of 0.198, and 0.218, and 0.927 mm/s for PAR30PE70, PAR50PE50, and PAR100 respectively. In hybrid rocket engine burning with oxygen, Tang *et al.* (2017) reported decrease in regression rate between 10% and 50% as the polyethylene mass fraction in paraffin increased from 1% to 10%. It seems possible, therefore, to find a mix of liquefying and polymeric fuels whose regression rate approaches that of pure polyethylene in a broad range of air mass flux. In the absence of such correlation, we suggest the coefficients a=0.069 and n=0.34, curve R7 in Fig. 1 for the numerical predictions. As it can be seen, the regression rate ($\dot{r}_7$) is a weak function of air mass flux in the range of 100 to 300 kg/m^{2}s. The blend would burn slightly faster than pure polyethylene and much lower than pure paraffin, but with improved fuel properties than the latter.

Paraffin-polyethylene blends have improved mechanical strength, higher density and melting temperature, and lower regression rate compared to pure paraffin. Depending on the mission and system requirements, paraffin-PE blend might be the primary choice for the solid fuel matrix for the propulsion of tactical missiles.

3. External and internal ballistics

3.1 Flight equations

Fig. 3 shows the main forces acting on a flight missile whose orthogonal frame is moving. The operational concepts and system architecture follow the aerodynamic, propulsion, and trajectory equations proposed by Fleeman (2012). The flight path estimation is based on a force balance, including thrust (T), drag (D), weight (W), and lift (L) applied to a material point, reducing the system to a two-degree of freedom. In Fig. 1, γ and α are, respectively, the flight path angle and missile angle of attack concerning the rocket axis. We assume that the flight trajectory changes with the help of control surfaces attached to the missile body, and the angle of attack (α) can attain values as high as 40 degrees (Lesieutre *et al.* 1987).

The flight path angle, therefore, changes accordingly. The system of equations of motion proposed by Campos *et al.* (2012) was adapted for missile systems. Missile velocity (V) and pitch

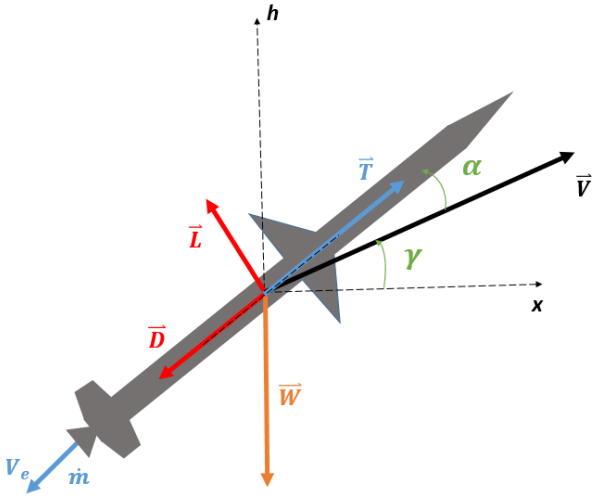

Fig. 3 Forces acting on a flying missile

angle (γ) are obtained after integrating the following equations

$$m(t)\frac{dV}{dt} = -W\sin(\gamma) - D\ \not{f}(\alpha) - L\sin(\alpha) + T\cos(\alpha) \tag{3}$$

$$m(t)V\frac{d\gamma}{dt} = -W\cos(\gamma) - Dr\sin + L\cos(\alpha) + T\sin(\alpha) \pm m(t)VK \tag{4}$$

Since the code is based on two degrees of freedom, rapid changes in pitch angle are accomplished by setting proper values to the constant K in Eq. (4).

The missile total propellant mass changes with time following

$$\frac{dm_p}{dt} = \frac{dm_{pb}}{dt} + \frac{dm_{pr}}{dt} \tag{5}$$

The rate of burning of the booster propellant is assumed to be constant; therefore, the booster propellant mass at time 't' is given by

$$m_{pb}(t) = m_{pb}(t_{i,b}) - \dot{c}_b(t - t_{i,b}) \tag{6}$$

for $t_{i,b} \leq t \leq t_{f,b}$. Outside this time range, the burning rate $\dot{c}_b$ is zero. The burning rate of the solid-fueled ramjet, however, may vary with time, then

$$m_{pr}(t) = m_{pr}(t_{i,r}) - 2\pi L_{fuel}\rho_{fuel}\frac{dr}{dt} \tag{7}$$

for $t_{i,r} \leq t \leq t_{f,r}$. Outside this time range, the ramjet burning rate is zero. In Eq. (7), $t_{i,r}$ is larger than $t_{f,b}$, meaning that ramjet ignition takes place only after booster thrust termination. Total mass of the missile is given by

$$m(t) = m_{db} + m_{dr} + m_p(t) \tag{8}$$

In Eq. (8), m_{db} and m_{dr} are the booster and ramjet dry masses. The former separates from the missile just after $t_{f,b}$.

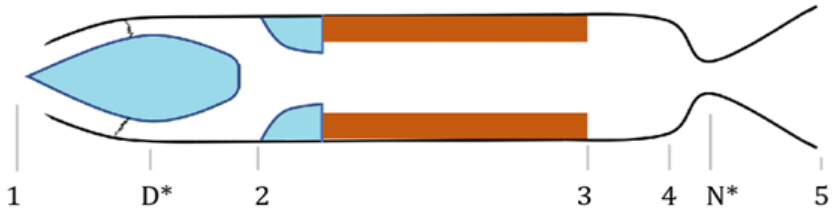

Fig. 4 Ramjet engine main stations

The missile altitude (h) and range (x) are inferred, respectively, by

$$\frac{dh}{dt} = V\sin(\gamma) \tag{9}$$

$$\frac{dx}{dt} = V\cos(\gamma) \tag{10}$$

In the equations of motion, weight, drag, lift and thrust are obtained, respectively, through

$$W = m(t)g \tag{11}$$

$$D = \frac{1}{2}C_d(\alpha)A_{ref}\gamma_{air}P_{air}M^2 \tag{12}$$

$$L = \frac{1}{2}C_n(\alpha)A_{ref}\gamma_{air}P_{air}M^2 \tag{13}$$

$$F = (\dot{m}_{air} + \dot{m}_{fuel})V_e - \dot{m}_{air}V_{cf} \tag{14}$$

$C_d(\alpha)$ and $C_n(\alpha)$ are the drag and lift coefficients, respectively. A_{ref} is the missile reference area, γ_{air} and P_{air} are, respectively, the air's specific heat ratio and static pressure, and M is the missile Mach number. V_e and V_{cf} are the nozzle exhaust and missile cruise flight velocities, respectively. Drag and lift correlation for the body, fins, and tail were extracted from Fleeman (2012). Wave, ram, and skin drag effects are computed from low subsonic to high supersonic flight.

3.2 Ramjet engine

Fig. 4 presents the main stations of a ramjet engine. Engine main parameters at different stations are obtained after solving a system of equations for mass and energy conservation, assuming ideal gas behavior and isentropic processes, respectively, by

$$\dot{m} = \rho_i V_i A_i \tag{15}$$

$$\sum q + \sum w = (h_{i+1} - h_i) + \frac{1}{2}(V_{i+1}^2 - V_i^2) \tag{16}$$

$$P_i = \rho_i R_{gas} T_i \tag{17}$$

Conservation of momentum is given by Eq. (14) and Mach number is calculated from the flow velocity and the local speed of sound using

$$M_i = \frac{V_i}{\sqrt{\gamma_i R_i T_i}} \tag{18}$$

In Eqs. (15)-(18), i refers to engine stations (1-5) as depicted in Fig. 4. The ramjet internal ballistics code follows that proposed by Struchtrup (2014).

3.2.1 Intake diffuser

An isentropic diffuser is considered in the current design to maximize the ramjet performance. For station i=1, pressure and temperature are obtained from the atmospheric condition at the missile flight altitude and velocity. Actual intake pressure recovery is obtained from (NASA 2022)

$$\frac{P_2}{P_1} = \eta_{int}(1 - 0.075(M-1)^{1.35}) \tag{19}$$

In Eq. (19), η_{int} is the intake efficiency.

3.2.2 Burner and nozzle

The combustion process is considered isobaric and material constraint limits the combustor exit gas temperature (T_3). The solid fuel combustion regime gives the combustor exit area (A_3), which should be dominated by convective heat transfer. At high mass flux, the flame may extinguish due to the small Damköhler number or strong lean combustion process resulting from an excess of oxidizer. Solid fuel burning must occur in the convective heat transfer regime. Energy conservation gives the total heat supplied by the combustor, and the exit burner temperature defines the combustor's overall equivalence ratio adjusting the (FA) ratio.

$$(FA)_{act} = \frac{\dot{m}_{fuel}}{\dot{m}_{air}} \tag{20}$$

The solid fuel mass flux, internal receding area, and density, combined with the average fuel regression rate help determine the fuel grain length

$$\dot{m}_{fuel} = \dot{r} A_{port} \rho_f \tag{21}$$

The thermodynamic states at the burner exit (station 3) define the inlet state of the nozzle (station 4). The stagnation temperature at station 4 is obtained from the balance of energy. The remaining thermodynamic conditions, at N^* and station 5, are obtained following the same steps used to define the diffuser's geometry (Struchtrup 2014).)

3.2.3 Solid booster

Booster size and thrust are calculate by the external ballistics code. Booster thrust and propellant burning rate are inferred, respectively, by

$$F_b = W(8g_0) \tag{22}$$

$$Isp_b = F_b/(c_b g_0) \tag{23}$$

Missile minimum acceleration was set to eight g's as in Eq. (22). Booster propellant mass is obtained from its burning time and rate. Operation time is that to bring the missile from rest to the cruise altitude and velocity. After inferring the mass of the propellant, dry booster mass is obtained from the following equation

$$PMF_b = m_{pb}/(m_{db} + m_{pb}) \tag{24}$$

The booster's specific impulse and propellant mass fraction depend on the system technology maturity. Brazil can produce solid fuel rockets whose propellant mass fraction is 83% with 270 s sea level specific impulse (da Cás *et al.* 2019).

3.3 Numerical solution and code validation

3.3.1 Internal and external ballistics codes

The system of equations was implemented in the Engineering Equation Solver (EES) platform. EES is an equation-solving program that handles thousands of coupled non-linear algebraic and differential equations (Klein and Nellis 2013). It also incorporates a high-accuracy thermodynamic and transport property database for hundreds of substances. The adjunct equations related to the thermodynamic state of the gases are obtained from the NASA polynomials for ideal gases stored in the internal function library of the EES platform. For numerical integration, EES uses a variant of the trapezoid rule along with a predictor-corrector algorithm (Klein and Nellis 2013). In EES, iteration halts when the relative residual of a variable is less than 10^{-6} or the change in variables during successive iterations falls below 10^{-9}. The solver saves the main parameters every second for post-processing mission profile analysis using the EES platform plot menu, including overlay plot capability for predicted performance comparison. The external and internal ballistics codes comprise 96 and 191 algebraic and differential equations, respectively. The solution to the initial value problems is provided through the following equation-based Integral function directive

$$F(t) = F(0) + Integral(dFdt;\ LowerLimit; UpperLimit; StepSize) \tag{25}$$

Drag and lift correlations at a given missile angle-of-attack are those listed in Fleeman (2012). All the coefficient equations were programmed as functions and procedures and stored in the EES external library. Drag and lift coefficients are obtained from call statements anywhere in the main code. Similar approach was taken for air density, static pressure, speed of sound, and temperature as a function of flying altitude. The atmospheric earth model (EAM 2022) infers thermodynamic properties with high accuracy up to 50,000 m altitude.

3.3.2 Ballistic codes validation

The internal ballistics code was validated by comparing ramjet engine predictions to those from a multi-platform tool designed for rocket engine analysis (Ponomarenko 2014). In the latter, the equilibrium composition of the combustion products is calculated minimizing the Gibbs free energy of the system for a broad range of rocket operating conditions. Table 1 gives the results from both methods for the combustion of hot air with paraffin wax ($C_{32}H_{66}$). As it can be seen, chamber thrust and effective velocity deviations from the proposed code to the equilibrium code are less than 2%. The chamber geometries are similar, with differences of less than 6.5%. Therefore, the internal ballistics code was deemed adequate for the preliminary design of solid fuel ramjet missiles.

The data of the Aerobee 150A sounding rocket and its mission profile were used to validate the external ballistics code. The vehicle is a four-fin sounding rocket, approximately 9.0 meters long and 38 cm in diameter, consisting of a solid rocket booster and a second stage (sustainer) based on a liquid propellant rocket engine. Comprehensive data on the Aerobee 150A is available in the NASA Technical Report R-226 (Busse and Leffler 1966). The platform was designed to carry

Table 1 Engine performance predictions comparisons

Input/output	Ramjet (Internal Ballistics Code)	RPA	Diff.
Chamber pressure (bar)	4.465	4.465	
Ambient pressure (bar)	0.2644	0.2644	
Inlet air temperature	500.4	500.4	
O/F ratio	26.1/1	26.1/1	
Gross Thrust (kN)	11.89	11.71	+1.52%
Nozzle throat diameter (mm)	156.2	164.76	-5.2%
Nozzle exit diameter (mm)	259.5	276.94	-6.3%
Effective exhaust velocity (m/s)	1,400	1,379	+1.54%

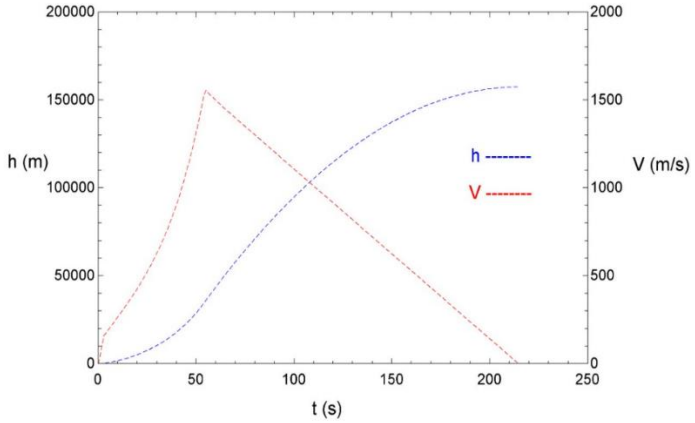

Fig. 5 External ballistics code predicted velocity and climbing profile of the Aerobee 150A sounding rocket

payloads of up to 136 kg to altitudes ranging from 120 to 300 km, depending on the transported mass. Sounding rockets like the Aerobee 150A were launched from the Wallops Island base in the USA. The long operating time of the Aerobee sustainer engine (51.5 s), compared to its booster (2.5 s), bears some resemblance to certain long-range missiles based on liquid ramjet technology, although with distinct mission profiles. The numerical solution predicted the maximum flight altitude reached by the Aerobee 150A as 156 km when transporting a 136 kg payload, as depicted in Fig. 5. This result closely aligned with the reported regular flights of the Aerobee, differing by less than 5% from the reported values (Busse and Leffler 1966). The external ballistics code was thus considered validated and deemed suitable for executing the preliminary missile design phase of long-range missiles.

4. System preliminary design

The top-level customer sets the missile requirements according to its specific needs and expected performance. Considering the Brazilian Navy is interested in new developments, and the country lacks similar systems in its inventory, the task must start with the definition of a basic missile configuration followed by an iterative designing process to improve the solution. Missile range, warhead mass, reference diameter, and flight program are predefined inputs from mission

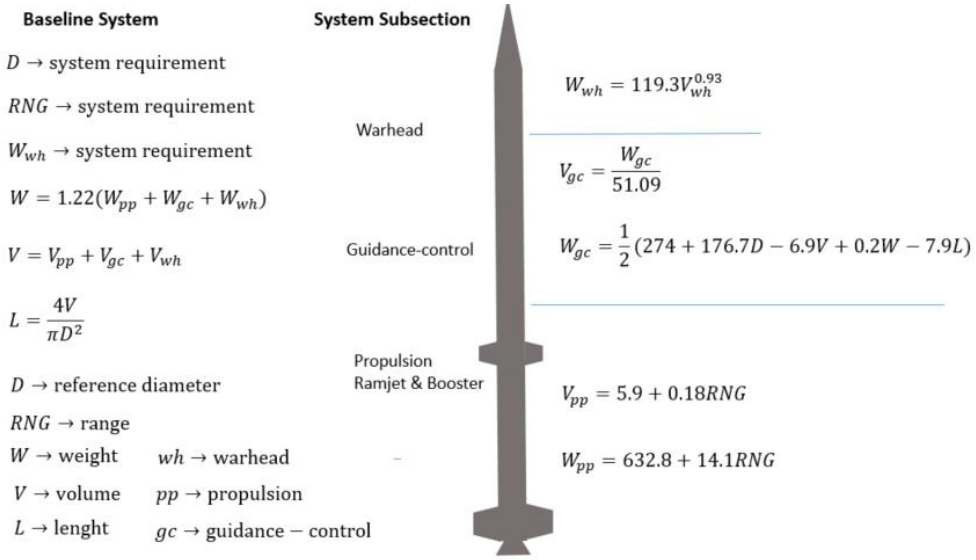

Fig. 6 Baseline missile subsection correlations (Nowell 1992)

requirements (Phase-0) as presented in Fig. 6. The baseline missile's subsections, masses, and geometries are calculated from published correlations available in Nowell (1992). The correlations in Fig. 6 are in Imperial units (lbm, ft) and the range (*RNG*) in nautical miles. Guidance-control mass was adjusted using the average mass of a large number of surface-to-surface missiles (274 lbm) and a total spectrum correlation (R^2=90%) where system diameter, volume, length, and mass are the independent variables (Nowell 1992). Auxiliary correlations were also employed for preliminary wing mass and area predictions for the booster and the sustainer, considering short and long-range missiles, respectively. Wing mass is negligible compared to the missile's total mass. Wing area, however, is relevant for overall system drag estimations.

As depicted in Fig. 5, overall missile mass (*W*) and geometry (*V*, *L*) are obtained by summing the estimated data from its main subsections, i.e., warhead (WH), guidance-control (GC), and propulsion (PP). Warhead and guidance-control subsections must be accommodated in 80% of the missile reference diameter allowing compressed air to flow-by and reach the ramjet combustor. The provision increases the length of the WH and GC subsections accordingly.

Fig. 7 shows the preliminary design flow chart. Phase-0 gives the missile reference diameter (*D*), warhead mass (*W*), flight altitude (*h*) and speed (*M*), and the expected range (*RNG*). Applying Nowell's correlations presented in Fig. 6, the baseline missile total mass, volume and length were calculated from its main subsections.

During system refinement, warhead and guidance-control masses and geometries are kept frozen. Therefore, the main objective of the code was to design the booster and ramjet sustainer engines able to carry out the prescribed system mission. The external ballistics code was then applied to size the booster thrust, dry, and propellant masses. Once the booster mass and geometry were calculated, the initial guess for the ramjet engine mass can be estimated. Preliminary ramjet mass was obtained subtracting the initial mass of the booster from the estimated total mass of the propulsion system from Nowell's correlations

$$m_r = W_{pp} - m_b \tag{26}$$

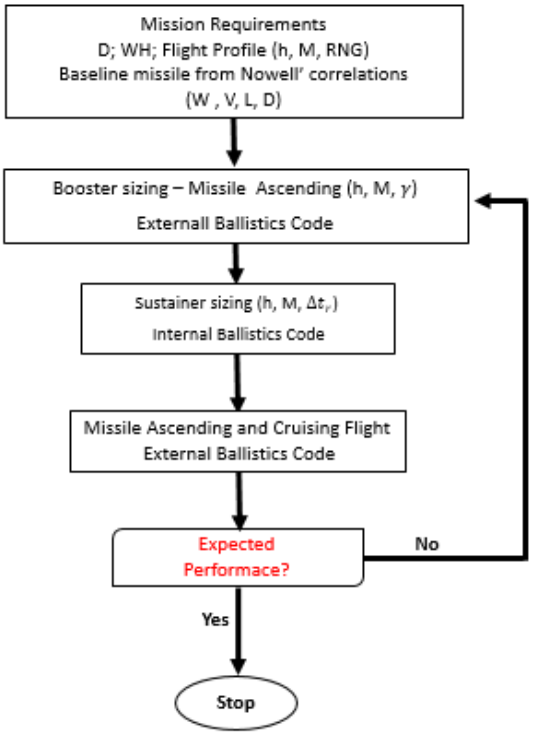

Fig. 7 Flow chart of the missile preliminary design

The sustainer thrust must overcome the total drag forces ($F=D$), which is a function of the system geometry, speed, and flight angle, while lift force must compensate the gravitational force ($L=G$) providing near-constant pitch flight angle ($d\gamma/dt\approx0$) throughout the cruise phase. The internal ballistics code performs ramjet engine sizing comprised of the solid-fueled grain, post-combustion chamber and main nozzle dimensions. Nozzle contraction area ratio was set to two followed by a conical exit nozzle with a 22° half-angle. A post-combustion section was included to increase the flue gases' residence time for improved combustion efficiency with a diameter-to-length ratio of two. Post combustion chamber is not needed when considering integrated rocket-ramjet configuration, as discussed earlier. Engine dry mass was estimated using the vessel thickness calculation method proposed by Buthod (2001). Ramjet intake area, solid-fuel initial and final diameters, and length were predicted by the internal ballistics code. Ramjet total drag was updated and the external ballistics code executed the missile ascending and cruising phases. Minor adjustments to the combined propulsion system are carried out, and the process was repeated until a converged solution was obtained. The process stops when the missile's total mass alteration is less than 1.0% between two successive refinements. During ascending, the ramjet intake is protected by a conical ogive, which must be ejected before the ramjet motor ignition. Cold booster separation takes place after its propellant mass is exhausted. For some required payload and flight profiles, total missile size and weight strongly rely on the geometry and mass of the combined propulsion system. Therefore, most of the effort in the search process is to determine the optimized sustainer propulsion volume and mass. In most cases, the preliminary design, as claimed by Phase-0, converges after few iterations. Some operational missiles help define the range of parameters for

Table 2 Engine performance predictions comparisons

Data	Baseline	1st	2nd	3rd
Total missile mass (kg)	2,092	2,092	2,116	2,128
Total missile length (m)	7.9	7.9	8.3	8.5
Inlet length (m)	-	0.5	0.5	0.5
Total ramjet length (m)	-	4.5	4.9	5.1
Ramjet engine length (m)	-	-	3.0	3.2
Warhead length (m)	0.64	0.64	0.64	0.64
GC length (m)	1.3	1.3	1.3	1.3
Booster length (m)	-	2.9	2.9	2.9
Warhead mass (kg)	200	200	200	200
GC (kg)	192	192	192	192
Propulsion mass (kg)	1,323	1,323	1,343	1,357
m_{pb} (kg)		908	908	908
m_{db} (kg)		186	186	186
m_{pr} (kg)		229	183	194
m_{dr} (kg)			66	69
Body structure mass (kg)	377	377	381	385
Missile density (kg/m^3)	934	934	942	890
$\Delta t_b/\Delta t_r$ (s)	-		14/293	14/296

preliminary technical and operational requirements of a tactical surface-to-surface missile, as follows:

Range-from 100 km to 300 km;
Flight regime-supersonic, up to Mach 3;
Launch weight-up to 3,000 kg;
Cruise altitude-10 to 20 km;
Diameter-less than 700 mm;
Warhead mass-from 100 to 300 kg of highly-explosive material (HE).

5. Results and discussion

We suppose the Brazilian Navy needs to develop a long-range surface-to-surface missile for 300 km range, carrying 200 kg of warhead, cruising at 14,000 m altitude at Mach 3, with 600 mm reference diameter. Nowell's correlations defined the subsections masses and geometries of the baseline missile, comprised of guidance-control (GC), warhead (WH), and propulsion (PP). Factor 1.22 in the mass equation accounts for additional weight from the missile structure, as recommended by Fleeman (2012). Table II presents the baseline system and the first three refinements following the preliminary design flow illustrated in Fig. 7. After running the external ballistics code, booster sizing and performance characteristics determine the first refined solution. The booster impulse places the missile at the designated altitude, Mach number, and pitch angle. Then, missile drag, including the share of the ramjet engine (ram-drag), can be estimated as a first guess to the ramjet sustainer thrust. A total drag force of 35.4 kN was obtained in the initial assessment. At the start of the cruising flight, the mass of the ramjet, comprised of propellant and

Table 3 Ramjet main parameters

Parameter	Station 1	Station 2	Station 4	Station 5
P (bar)	0.142	3.682	3.462	0.142
T (K)	216	601.6	1,679-1,384	547.4
$\dot{m}$ (kg/s)		28.78	29.453	
D (mm)	426	600	600	564
Mach	3	0.2	0.17	2.8
F (kN)				17-13
F_{gross} (kN)				42-38
Isp (s)				1,847-1,967

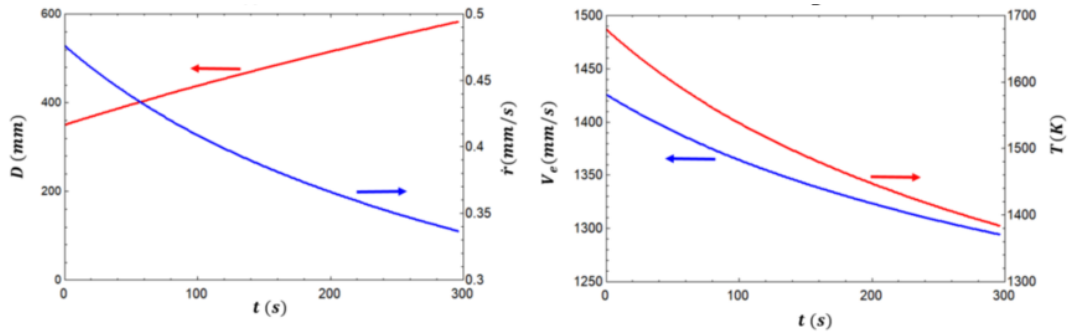

(a) (b)

Fig. 8 Fuel regression rate, grain port diameter, exhaust velocity, and burner exit temperature during cruise flight

structure, was set to 229 kg, obtained by subtracting the booster mass (1,094 kg) from the baseline missile initial mass (1,323 kg).

Ramjet thrust depends on the air intake area and the combustion parameters. The dynamic evolution of the solid fuel port diameter sets the maximum engine operation time as the grain port approaches the missile reference diameter (600 mm). Increased burning times can be attained reducing the initial port diameter as long as the air mass flux does not exceed 350 kg/m^{2}s. Booster and the ramjet burning times were 14 and 296 seconds, respectively (Table 2). For the ramjet, the maximum combustion products temperature was set to 1,700 K to avoid expensive materials for the post-combustion chamber and nozzle. The internal ballistics code gives the solid fuel and total engine lengths and masses. For that, the calorific value and density of the solid-fuel were set to 42,150 kJ/kg and 910 kg/m^3, respectively.

After pre-sizing the ramjet engine, the external ballistics code is executed again to update the booster engine parameters and the initial cruising flight drag. As shown in Table II, the sizing of the booster converged after the first refinement since the mass of the ramjet engine went through minor changes due to the good propulsion mass estimate from Nowell's correlation. To some degree, that was fortuitous. For example, applying the correlations (Fig. 6) to the MGM-52 Lance long-range missile (Lance 2023), the difference in total mass between the baseline predictions and the actual system was less than 7.5%. However, for the propulsion subsection, the difference in mass prediction was 31%. The actual propulsion mass of the Lance was 1,021 kg, and the model predicted 702 kg. In any case, a converged solution can always be obtained after a few

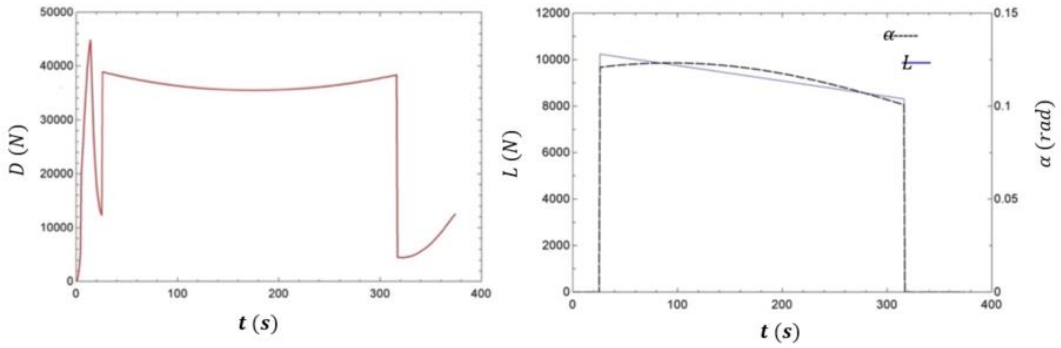

(a) (b)

Fig. 9 Time variation of drag force (A); lift force and missile angle of attack (B)

adjustments.

Following booster separation, the ramjet missile was 5,100 mm long, weighing 1,038 kg, flying with 194 kg paraffin-polyethylene fuel. Table 3 presents relevant parameters for the solid-fueled ramjet engine. The efficiency of the isentropic intake was set to 90%, leading to 72.8% stagnation pressure recovery, or 368 kPa at station 2 (Fig. 3). The ramjet intake area of 0.1425 m^2 captured 28.8 kg/s of air for the combustor, which provided 15 kN of average net thrust.

Fig. 8 (a) shows the instantaneous fuel regression rate and solid fuel grain port diameter and Fig. 8 (b) shows the exhaust velocity and burner exit temperature throughout the cruise flight for a fixed grain length of 1,900 mm. The port diameter varied from 350 to 582 mm causing engine mass flux to vary from 299 to 108 kg/m^2s. The change in mass flux altered the fuel regression rate, that ranged from 0.48 to 0.34 mm/s. For a fixed air mass flow rate, the reduction in the fuel-to-air ratio decreases the burner exit temperature (1679-1384 K), nozzle exhaust velocity (14126-1294 m/s), and engine gross thrust (42-38 kN). The averaged fuel burning rate and fuel-to-air ratio were 2,853 kg/h and 0.0312, respectively. In this preliminary assessment, the fuel regression rate decreases as the grain port increases, causing alterations on the overall fuel-to-air ratio.

The required ramjet sustainer thrust, shown on Fig. 9 (a), must compensate the total system drag forces whose main contributions are from the motor itself, along with those related to variations in the missile angle of attack. During cruise flight, drag forces varied from 38.8 to 38.3 kN. Along the cruise phase, gravitational forces are compensated through lift obtained by adjusting the missile angle of attack, as shown in Fig. 9 (b). Lift forces varied from about 10.3 to 8.3 kN for an average missile angle of attack of about 6.3 degrees (0.11 rad). Missile lift increases drag, which, in turn, claims higher thrust. The coupling of these counterbalanced forces sets the missile pitch and angle of attack for near-constant flight altitude. The missile flight profile comprised a rapid ascending (~20 s), cruising (~300 s) and descending. (~40 s) phases. Booster impulse brought the system to the required flight altitude, velocity, and near zero pitch angle in less than 40 s. Booster cold separation took place 15 s after take-off when the missile reached Mach 3.7, decaying to the desired cruise speed by the action of the drag forces. A rapid adjustment in pitch angle was provided by setting a proper value to the constant K in Eq. (4). The nose cone is ejected and the ramjet missile engine fired up, burning for about 296 s. The non-powered descending phase starts after 340 s from the time of launch. The missile can reach a target more than 300 km from its launch location at a steep angle and Mach 1.64.

The influence of the fuel composition on regression rate and mission performance was further

investigated taking the correlations listed in Fig. 1, for pure polyethylene and pure paraffin. For 100% PE fuel, the grain length should increase to 3,200 mm due to the lower regression rate range (0.26-0.20 mm/s) throughout motor operation (296 s). The initial and final grain diameters were estimated as 350 and 484 mm for the current mission. Ramjet engine fuel length increased by 38% to counterbalance the much lower regression rates, as compared to the PARPE blend ($\dot{r}_7$). The ramjet propellant mass fraction for this configuration was estimated as 67%, which is lower than that for the paraffin-polyethylene blend. Ramjet engine mass increased 27 kg, as a result of the additional 1,200 mm in the length of the motor.

A higher regression rate fuel would decrease motor length, fuel burning time, and missile range. For instance, applying the ballistics coefficients of Azevedo *et al.* (2019), the regression rate of pure paraffin varied from 2.0 to 1.4 mm/s for mass flux of 299-101 kg/m^{2}s. The maximum allowed fuel grain diameter (~600 mm) was reached after 79 s of motor operation, greatly decreasing missile range, for an initial diameter of 350 mm. To give the target motor combustion temperature, the grain length was only 460 mm. Therefore, apart from structural concerns, pure paraffin seems not adequate for long-range missile applications.

Finally, we investigated the use of bypass provision to keep the motor *FA* ratio constant during cruise flight. Fixed regression rate can be narrowly attained with constant grain port oxidizer mass flux. The latter can be achieved bypassing the core air with a flow control device. Numerical predictions were then carried out by the internal ballistics code for the fixed regression rate strategy using the ballistics coefficients from $\dot{r}_7$ (PARPE blend). For constant regression rate of 0.3 mm/s, achieved with 77 kg/m^{2}s of air mass flux, the fuel length would have 2,150 mm to maintain the required overall (*FA*) ratio and motor net thrust (38 kN). For that, the bypass ratio varied from 74 to 27% and grain diameter reached 590 mm, after 400 s of operation. This additional burning time would increase missile range in excess of 90 km. The system, however, would claim room for air to pass around the fuel grain, decreasing its final diameter and burning time. Adopting lateral squared air intakes, similar to the French ASMP-A missile (ASMP 2022), and integrated rocket-ramjet engine, the final grain diameter can approach that of the reference missile (600 mm). Such configuration increased ramjet propellant mass fraction to 78%.

6. Conclusions

In this paper, we have presented a comprehensive set of tools for the preliminary design phase of an anti-ship supersonic missile propelled by a ramjet engine based on liquefying fuels. The proposed method enabled the determination of the system's fundamental configuration, incorporating the main missile subsystems, namely guidance-control, warhead, and combined propulsion. Starting from a baseline missile that was pre-sized using published correlations, the iterative process facilitated the refinement of the booster and ramjet sustainer engines to meet a range of missile requirements. The combination of these tools yielded a preliminary long-range surface-to-surface missile, 600 mm in diameter, capable of carrying a 200 kg warhead to distances exceeding 300 km. The refined final weight was calculated to be 2,128 kg, which reduced to 1,034 kg after booster separation. The ramjet sustainer was designed to fly at Mach 3, 14,000 m altitude. Overall ramjet density and propellant mass fraction were estimated as 890 kg/m^3 and 74%, respectively. To further increase the range, we propose incorporating lateral intake and variable air mass flow rate, while maintaining a constant fuel regression rate using a paraffin-polyethylene blend.

Acknowledgments

The authors are grateful for the technical support of collaborators of the Chemical Propulsion Laboratory of the University of Brasilia. Also, this study was financed in part by the Coordenação de Aperfeiçoamento de Pessoal de Nível Superior-Brasil (CAPES)-Finance Code 001.

References

Air-Sol Moyenne Portée-Wikipedia (2023), Air-Sol Moyenne Portée, Wikipedia Foundation, St. Petersburg, USA.

ASTROS (2014), ASTROS 2020 MLRS: Brazil's Industrial Investment in Precision Strike, Defense Industry Daily, Vermont, USA.

Azevedo, V.A., Alves, I. and Shynkarenko, O. (2019), "Experimental investigation of high regression rate paraffin for solid fuel ramjet propulsion", *Proceedings of the AIAA Propulsion and Energy 2019 Forum*, Indianapolis, USA, August.

Bertoldi, A.E.M., Veras, C.A.G., Shynkarenko, O., Andrianov A., Lee, J. and Domenico, S. (2022), "Overview of the past and current research on hybrid rocket propulsion at the University of Brasília", *Proceedings of the 9th European Conference for Aeronautics and Space Sciences (EUCASS)*, Lille, France, June.

Busse, J.R. and Leffler, M.T.A (1996), "Compendium of aerobee sounding rocket launchings from 1959 through 1963", NASA Technical Report TR R-226, Goddard Space Flight Center, Greenbelt, USA.

Buthod, P. (2001), *Pressure Vessel Handbook*, Pressure Vessel Publishing INC., Tulsa, OK, USA.

Campos, L.M.B.C. and Gil, P.J.S. (2018), "On four new methods of analytical calculation of rocket trajectories", *Aerosp.*, **5**(3), 88. https://doi.org/10. 3390/aerospace5030088.

da Cás, P.L., Veras, C.A., Shynkarenko, O. and Leonardi, R. (2019), "A Brazilian space launch system for the small satellite market", *Aerosp.*, **6**(11), 123. https://doi.org/10.3390/aerospace6110123.

da Cás, P.L.K. and Veras, C.A.G. (2012), "An optimized hybrid rocket motor for the SARA platform reentry system", *J. Aerosp. Technol. Manage.*, **4**(3), 317-330. https://doi.org/10.5028/jatm.2012.04032312.

Decreto n. 6.703 (2008), Aprova a Estratégia Nacional de Defesa, Presidência da República, Brasília, Brazil. https://www.planalto.gov.br/ccivil_03/_ato2007-2010/2008/decreto/d6703.htm.

Dutta, D. (2014), "Probabilistic analysis of anti-ship missile defence effectiveness", *Def. Sci. J.*, **64**(2), 123-129. https://doi.org/10.14429/dsj.64.3532.

EAM (2021), Earth Atmosphere Model, NASA, Cleveland, USA.

ECSS (2017), System Engineering General Requirements; European Cooperation for Space Standardization, Noordwijk, The Netherlands. https://ecss.nl/standard/ecss-e-st-10c-rev-1-system-engineering-general-requirements-15-february-2017/

Fleeman, E. (2012), *Missile Design and System Engineering*, American Institute of Aeronautics and Astronautics, Inc, Reston, VA, USA.

Garcia, A., Yamanaka, S.S.C., Barbosa, A.N., Bizarria, F.C.P., Jung, W. and Scheuerpflug, F. (2011), "VSB-30 sounding rocket: History of flight performance", *J. Aerosp. Technol. Manage.*, **3**, 325-330.

Karabeyoglu, A., Zilliac, G., Cantwell, B.J., DeZilwa, S. and Castellucci, P. (2004), "Scale-up tests of high regression rate paraffin-based hybrid rocket fuels", *J. Propuls. Power*, **20**(6), 1037-1045. https://doi.org/10.2514/1.3340.

Karabeyoglu, M.A., Altman, D. and Cantwell, B.J. (2002), "Combustion of liquefying hybrid propellants: Part 1, General theory", *J. Propuls. Power*, **18**(3), 610-620. https://doi.org/10.2514/2.5975.

Kim, S., Moon, H., Kim, J. and Cho, J. (2015). "Evaluation of paraffin-polyethylene blends as novel solid fuel for hybrid rockets", *J. Propuls. Power*, **31**(6), 1750-1760. https://doi.org/10.2514/1.B35565.

Klein, S.A. and Nellis, G. (2013), Mastering EES, f-Chart Software, Madison, MI, USA.

Lesieutre, D., Mendenhall, M., Nazario, S. and Hemsch, M. (1987), "Aerodynamic characteristics of

cruciform missiles at high angles of attack", *Proceedings of the 25th AIAA Aerospace Sciences Meeting*, Reno, United States, March.

Li, W., Chen, X., Zhao, D., Wang, B., Ma, K. and Cai, T. (2020), "Swirling effect on thermodynamic performance in a solid fueled ramjet with paraffin-polyethylene", *Aerosp. Sci. Technol.*, **107**, 106341. https://doi.org/10.1016/j.ast.2020.106341.

Martos, J.F.A., Rêgo, I.S., Laiton, S.N.P., Lima, B.C., Costa, F.J. and Toro, P.G.P. (2017), "Experimental investigation of Brazilian 14-XB hypersonic scramjet aerospace vehicle", *Int. J. Aerosp. Eng*., **2017**, Article ID 5496527. https://doi.org/10.1155/2017/5496527.

MGM-52 (2023), MGM-52 Lance, Wikipedia Foudantion, Inc., San Francisco, USA. https://en.wikipedia.org/wiki/MGM-52_Lance

NASA (2021), Inlet Performance, National Aeronautics and Space Administration, Cleveland, USA.

Neiva, R.Q. (2016), "Técnica de otimização aplicada em projeto conceitual de mísseis táticos", M.Sc. Thesis, University of Brasilia, Brasilia.

Nowell Jr., J.B. (1992), "Missile total and subsection weight and size estimation equations", M.Sc. Thesis, Naval Postgraduate School, Monterrey.

Ponomarenko, A. (2014), "RPA-Tool for rocket propulsion analysis", *Proceedings of the Space Propulsion Conference*, Cologne, Germany, May.

Sidhu, W.P.S. (2007), *Looking Back: The Missile Technology Control Regime, Arms Control Today*, April.

Struchtrup, H. (2014), *Thermodynamics and Energy Conversion*, Springer, Berlin, Germany.

Tang, Y., Chen, S., Zhang, W., Shen, DeLuca, L.T. and Ye, Y. (2017), "Mechanical modifications of paraffin-based fuels and the effects on combustion performance", *Propell. Explos. Pyrotech.*, **42**, 1268.1277. https://doi.org/10.1002/prep.201700136.

Turns, S.R. (2011), *An Introduction to Combustion*, McGraw-Hill Education, Godfrey, IL, USA.

AP